Publishing House
AKAPIT

COMPUTER METHODS IN MATERIALS SCIENCE

Informatyka w Technologii Materiałów

Vol. 15, 2015, No. 1

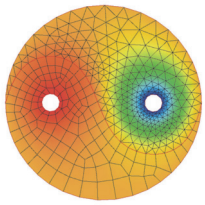

EVALUATION OF MACROSCOPIC STRESSES IN DISCRETE ELEMENT MODELS OF SINTERING PROCESSES

JERZY ROJEK[1]*, SZYMON NOSEWICZ[1], KATARZYNA PIETRZAK[1,2], MARCIN CHMIELEWSKI[2]

[1] Institute of Fundamental Technological Research (IPPT PAN), Pawińskiego 5B, 02-106 Warszawa, Poland
[2] Institute of Electronic Materials Technology, Wólczyńska 133, 01-919 Warszawa, Poland
**Corresponding author: Jerzy.Rojek@ippt.pan.pl*

Abstract

This paper presents investigation of macroscopic stresses in powder metallurgy process modelled with the discrete element method. The discrete element model belongs to the class of micromechanical models. In the DEM model the material is represented by an assembly of particles interacting by contact forces and the method is formulated in terms of forces and displacements. In order to evaluate macroscopic stresses a special upscaling procedure is necessary.

The paper presents basic formulation of the discrete element method with special attention for the contact interaction models for powder compaction and sintering. A method to evaluate macroscopic stresses based on the two level averaging is presented. The discrete element model of sintering is verified using own experimental results. Macroscopic stresses are calculated for the whole process including loading, heating, sintering, cooling and unloading. It has been found out that the macroscopic stresses are consistent with changing process parameters. The procedure is suitable for multiscale modelling of sintering.

Key words: sintering, modeling, discrete element method, macroscopic stresses

1. INTRODUCTION

Sintering is an essential stage of powder metallurgy processes in which solid parts are manufactured from metal or ceramic powder mixtures. Sintering consists in consolidation of loose or weakly bonded powders at elevated temperatures, close to the melting temperature with or without additional pressure. Sintering is a complex process affected by many factors and sensitive to many defects. Some of the most frequent defects such as cracks and shape distortions are associated with stresses during and after the sintering process.

Numerical modelling can be employed to simulate a sintering process and analyse sintering stresses and shape distortion of sintered parts. There are different approaches in modelling of sintering processes, ranging from continuum phenomenological models to micromechanical and atomistic ones.

This work presents application of the discrete element method (DEM) to modelling of sintering. The discrete element model belongs to the class of micromechanical models. In the DEM model the material is represented by an assembly of particles interacting by contact forces. The discrete element model of sintering requires a special interaction model. This work employs an original viscoelastic model developed by Nosewicz et al. (2013).

Numerical simulation of sintering at the microscopic level allows us to study material phenomena occurring during sintering, such as interaction between the grains during sintering and their rearrangement, material shrinkage and gradual decrease of porosity. Use of an averaging procedure will al-

 ISSN 1641-8581

low us to transfer force-type interactions to macroscopic stresses.

2. SINTERING MECHANISMS

During sintering, a particulate material (figure 1) is converted into a solid compact body (Olevsky, 1998). In the initial stage, cohesive bonds (necks) are formed between grains. Microstructure at an early stage of sintering is shown in figure 2a. When the sintering process is continued the necks between particle grow. Grain rearrangement and increase of grain compaction can be observed during sintering (figure 2b).

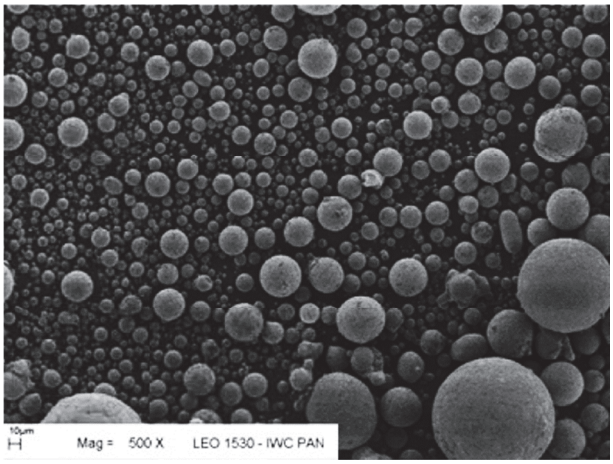

Fig. 1. *Morphology of the NiAl powder.*

3. NUMERICAL MODEL OF SINTERING

Numerical model of sintering used in the present work has been developed within the framework of the discrete element method which assumes that a particulate material can be represented as a collection of spherical particles interacting among one another, thus the discrete element model takes explicitly into account the particulate nature of the sintered material (Nosewicz et al., 2013). The numerical model of sintering has been implemented in the finite/discrete element code DEMPack (Dempack, 2013).

3.1. Discrete element formulation

In the discrete element method, the motion of rigid spherical elements (particles) is governed by the standard equations of rigid body dynamics. In general, both the translational and rotational motion is considered in Rojek et al. (2005). Here, however, we have neglected the tangential interaction between particles, similarly as in Martin et al. (2006), therefore the rotational motion of the particles is not considered. This favors particle compaction. Thus, the translational motion of the *i*-th particle is described by the equation:

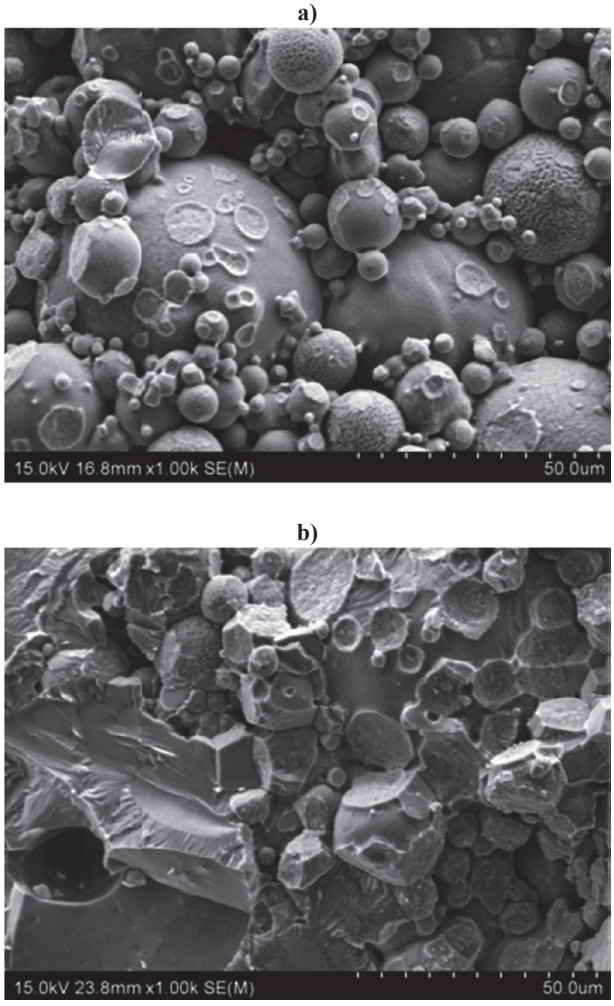

Fig. 2. *Microstructure evolution during sintering of the NiAl: early stage of sintering (a), late stage of sintering (b).*

$$m_i \ddot{\mathbf{u}}_i = \mathbf{F}_i , \tag{1}$$

where $\mathbf{u}_i$ is the element centroid displacement in a fixed (inertial) coordinate frame $\mathbf{X}$, m_i – element (particle) mass, and $\mathbf{F}_i$ – resultant force. The force vector $\mathbf{F}_i$ includes all the forces applied to the ith element due to external load, $\mathbf{F}_i^{\text{ext}}$ and contact interactions with neighbouring spheres and boundary surfaces $\mathbf{F}_{ij}^{\text{cont}}$, $j = 1, \ldots, n_i^c$, where n_i^c are the number of elements being in contact with the i-th discrete element

$$\mathbf{F}_i = \mathbf{F}_i^{\text{ext}} + \sum_{j=1}^{n_i^c} \mathbf{F}_{ij}^{\text{cont}}. \tag{2}$$

Contact forces $\mathbf{F}_{ij}^{\text{cont}}$ are obtained using a suitable constitutive model formulated for the interaction

of two particles. The present model employs two different interaction models for different stages of the process, one model for the compaction stage and the other for sintering.

3.2. Contact model for powder compaction

Powder compaction prior to sintering is modeled assuming cohesionless and frictionless contact conditions. The rheological scheme of this model is shown in figure 3.

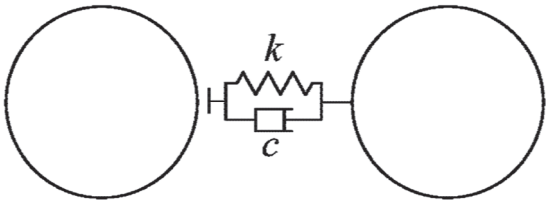

Fig. 3. *Rheological scheme of the contact interaction for powder compaction.*

The contact interaction is represented by the Kelvin-Voigt element consisting of a spring and a dashpot connected in parallel. The total contact force F_n is a sum of the elastic force in the spring F_n^e and the viscous component F_n^d

$$F_n = F_n^e + F_n^d. \tag{3}$$

The elastic part of the normal contact force F_n^e can be evaluated assuming a linear force–displacement relationship

$$F_n^e = k_n u_{rn}, \tag{4}$$

where k_n is the contact stiffness and u_{rn} is the penetration of the two particles, calculated as

$$u_{rn} = d_{ij} - r_i - r_j, \tag{5}$$

where d_{ij} is the distance of the particle centres, and r_i, r_j their radii.

No cohesion is allowed, so no tensile normal contact forces are allowed

$$F_n^e \le 0. \tag{6}$$

The viscous component of the normal force is assumed to be a linear function of the normal relative velocity v_{rn}

$$F_n^d = c_n v_{rn} \tag{7}$$

where

$$v_{rn} = (\dot{\mathbf{u}}_j - \dot{\mathbf{u}}_i)\cdot \mathbf{n}_i. \tag{8}$$

The value of the viscosity coefficient c_n can be taken as a fraction ξ of the critical damping C_{cr} for the system of two rigid bodies with masses m_i and m_j, connected with a spring of the stiffness k_n

$$c_n = \xi\, C_{cr} \tag{9}$$

where the critical damping can be calculated as, cf. Taylor and Preece (1992):

$$C_{cr} = 2\sqrt{\frac{m_i m_j k_n}{m_i + m_j}}. \tag{10}$$

3.3. Contact model for sintering

Contact interaction during sintering is represented by an original viscoelastic model developed by Nosewicz et al. (2013). The rheological scheme of this model is shown in figure 4. The model consists of two parallel elements, one representing the sintering driving force F^{sint} and the other being the Maxwell element comprising the elastic component in series with the viscous one.

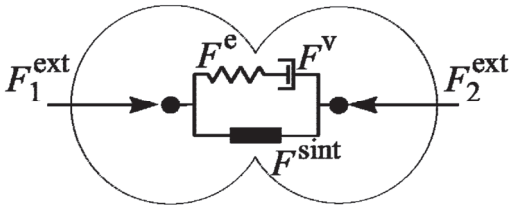

Fig. 4. *Rheological scheme of the contact interaction during sintering.*

For the Maxwell element, we have the following relationships for forces and velocities:

$$F^v = F^e \tag{11}$$

$$v_{rn} = v^v{}_{rn} + v^e{}_{rn} \tag{12}$$

Equation (11) means that the forces transferred through the spring and viscous component, F^e and F^v, respectively, are equal. Equation (12) expresses the additive decomposition of the relative normal velocity between particles v_{rn} into the elastic and viscous parts, $v^e{}_{rn}$ and $v^v{}_{rn}$, respectively.

The elastic force is expressed by the linear relationship

$$F^e = k_n u^e{}_{rn} \tag{13}$$

where k_n is the contact stiffness and $u^e{}_{rn}$ is the elastic part of the relative normal displacement at the contact point. The viscous force is written in the form:

$$F^v = \eta v^v{}_{rn} \tag{14}$$

where η is the viscosity coefficient. Substituting equations (14) and (13) into (12) we obtain the evolution equation for the force in the Maxwell branch

$$v_{rn} = \frac{\dot{F}^e}{k_n} + \frac{F^e}{\eta} \tag{15}$$

The sintering driving force and viscosity are evaluated according the the classical models developed for two-particle sintering (Coble, 1961; Johnson, 1969; De Jonghe & Rahaman, 1988) and used in previous implementations in the discrete element method, cf. Parhami and McMeeking (1998), Martin et al. (2006), Olmos et al. (2009). The sintering driving force F^{sint} and viscosity coefficient η are given by the following formulae:

$$F^{sint} = \pi\gamma_S\left[4r\left(1-\cos\frac{\Psi}{2}\right)+a\sin\frac{\Psi}{2}\right] \tag{16}$$

$$\eta = \frac{\pi a^4}{8D_b} \tag{17}$$

where r – the particle radius, a – the radius of the interparticle grain boundary, Ψ – the dihedral angle, γ_S – the surface energy and D_b – the effective grain boundary diffusion coefficient. The geometrical parameters of the model are defined in figure 5.

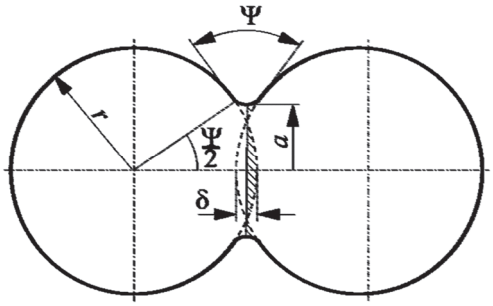

Fig. 5. *Two-particle model of sintering.*

The effective diffusion coefficient is given by the following equation, cf. Parhami and McMeeking (1998):

$$D_b = \frac{D_g \delta_g \Omega}{kT} \tag{18}$$

where D_g – diffusion coefficient, δ_g – thickness of the grain bound ary, Ω – atomic volume, k – Boltzmann constant, T – sintering temperature.

4. EVALUATION OF MACROSCOPIC STRESSES

The discrete element model presented in this work can be used in the framework of multiscale modelling of sintering as the model at microscopic level (Pan, 2003). Multiscale analysis requires transfer of the parameters between scales. Transition between scales can be performed two ways, from the lower scale to the upper one (this is called upscaling) or from the upper scale to the lower one (downscaling).

The transfer can be applied to different types of parameters. In this work special attention is paid to the micro-macro transition (upscaling) involving macroscopic stresses and microscopic forces.

Theoretical bases of upscaling have been developed within the theory of homogenization which was also applied to granular materials modelled with the discrete element method (Kruyt & Rothenburg, 2004; Kruyt & Rothenburg, 1998). In this work, The macroscopic stress tensor will be determined using the concept of two-level averaging procedure presented in Chang et al. (1995), Luding (2004).

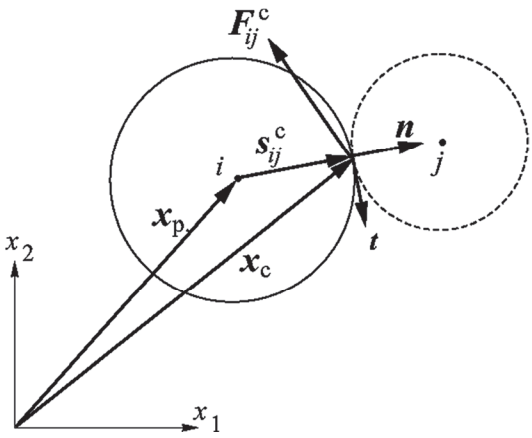

Fig. 6. *Definition of inter-particle interaction.*

We assume that the discrete elements (figure 6) interact among themselves with contact forces determined according to the model described earlier, being the material model at the microscopic scale. In the first stage we perform averaging over the representative volume elements coinciding with discrete elements volumes V_p. Thus we obtain the quantity Q represented by the constant value Q_p over the volume of the p-th discrete element. In the second stage we perform averaging over representative volumes containing a certain number of discrete elements.

The stress tensor σ_p for a single discrete element will be calculated by averaging over the element volume V_p

$$\sigma_p = \frac{1}{V}\int_{V_p} \sigma \, \mathrm{d}\Omega \tag{19}$$

Using the equilibrium condition and divergence theorem the volume integral (19) can be transformed into the surface one (Luding, 2004):

$$\sigma_p = \frac{1}{V_p}\int_{S_p} \mathbf{x}\mathbf{q} \, \mathrm{d}S \tag{20}$$

where $\mathbf{q} = \sigma \cdot \mathbf{n}$ is the stress vector, with $\mathbf{n}$ being the unit vector normal to the element surface S_p (cf. figure 6). Taking into account that the surface loading in our case is produced by concentrated forces $\mathbf{F}^c$ the surface integral in equation (20) can be written as the following sum (Chang et al., 1995; Luding, 2004):

$$\sigma_p = \frac{1}{V_p}\sum_{c=1}^{n_{pc}} \mathbf{x}_c \mathbf{F}^c \tag{21}$$

where n_{pc} is the number of elements being in contact with the p-th element. Writing the position vector of the contact point $\mathbf{x}_c$ as the sum of the position vector of the element center, $\mathbf{x}_p$, and the vector, $\mathbf{s}^c$, connecting the element center with the contact point

$$\mathbf{x}_c = \mathbf{x}_p + \mathbf{s}^c \tag{22}$$

for the static equilibrium we obtain the stress tensor for a single discrete element in the following form:

$$\sigma_p = \frac{1}{V_p}\sum_{c=1}^{n_{pc}} \mathbf{s}^c \mathbf{F}^c \tag{23}$$

After calculation of stresses for single elements σ_p, we can perform averaging over representative volume elements, defined for any point $\mathbf{x} \in \Omega$. Given constant stresses over elements, the average stress in the representative volume element can be calculated as, cf. Chang et al. (1995), Luding (2004):

$$\overline{\sigma} = \langle \sigma \rangle = \frac{1}{V}\sum_{p \in V} V_p \sigma_p = \frac{1}{V}\sum_{p \in V}\sum_{c=1}^{n_{pc}} \mathbf{s}^c \mathbf{F}^c . \tag{24}$$

The expression (24) for the mean stress of a representative volume can be written in an alternative equivalent form, cf. Chang et al. (1995):

$$\overline{\sigma} = \frac{1}{V}\sum_{c=1}^{N_c} \mathbf{L}^c \mathbf{F}^c \ , \tag{25}$$

in which summation is over all N_c contacts in the representative volume element and $\mathbf{L}^c$ is the so called branch vector connecting the centroids of two particles, for two particles i and j defined as follows

$$\mathbf{L}^c_{(ij)} = \mathbf{x}_p^{(i)} - \mathbf{x}_p^{(j)} \tag{26}$$

where $\mathbf{x}_p^{(i)}$ and $\mathbf{x}_p^{(j)}$ are the position vectors of the two particle centroids.

5. EXPERIMENTAL STUDIES OF SINTERING

Experimental studies of sintering have been has been carried out for NiAl powder. Morphology of the NiAl powder used for sintering is presented in figure 2. Sintering has been performed under pressure of 30 MPa and at temperature of 1400°C. Temperature and pressure variation during the process are plotted in figure 7. The samples of the sintered material are shown in figure 8. The process was interrupted at different time instants in order to study the evolution of microstructure and density during sintering. The density evolution, strictly related to sintering kinetics, was used in the validation of the developed numerical models of sintering.

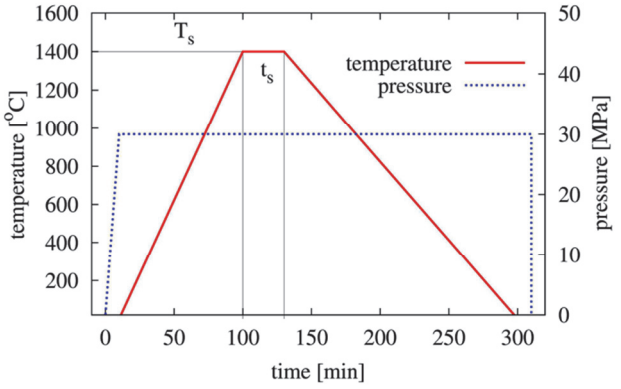

Fig. 7. Pressure and temperature profiles.

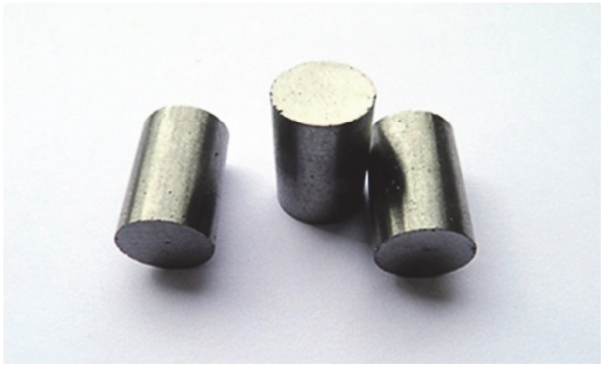

Fig. 8. Sintered specimens.

6. NUMERICAL RESULTS

Maintaining the original grain size and grain size distribution, a cylindrical container of diameter 200 μm has been filled with 1751 particles (figure 9a). It has been assumed that such a reduced geometric model represents correctly sintering process in a real specimen with diameter of 120 mm. This assumption is justified provided the parameters characterizing sintering are uniformly distributed in a real specimen volume. The model parameters used in the analysis are given in table 1. The whole process consisting of loading, heating, sintering, cooling and unloading has been simulated using the pressure and temperature profiles shown in figure 7. Figure 9b shows the final geometry of the sintered specimen. A significant height reduction can be observed. Density evolution during sintering is plotted in figure 10. It can be observed that numerical results are in quite a good agreement with experimental data.

Table 1. *Material data for NiAl sintering.*

Material constant	Parameter value
Diffusion coefficient, $D_g\delta_g$	$1.85 \cdot 10^{-20}$ m^3/s
Atomic volume, Ω	$1.20 \cdot 10^{-29}$ m^3
Surface energy, γ_s	1.57 J/m^2
Dihedral angle, Ψ	129^o
Density, ρ	5910 kg/m^3

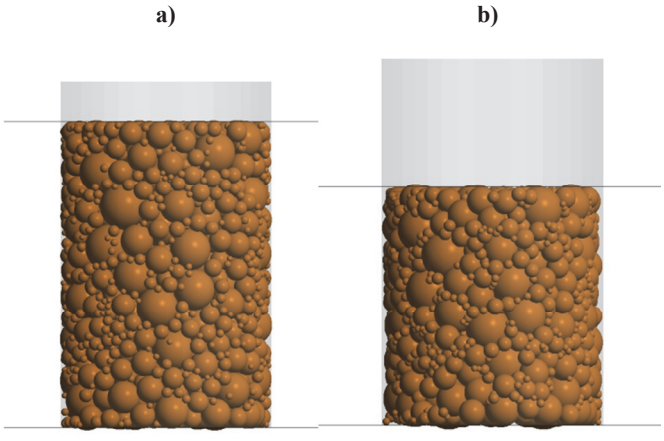

Fig. 9. *DE model of NiAL sintering: initial geometry (a), final geometry (b).*

Macroscopic average stresses have been calculated using the procedure presented in chapter 4. The whole specimen has been treated as the RVE. Evolution of the macroscopic stresses during the whole process is plotted in figures 11 and 12. It can be seen in figure 11 that the axial stresses are in equilibrium with externally applied pressure during nearly all the process except for the initial stage of sintering. This is reasonable since at this stage the system undergoes the most intensive compaction. Evolution of the three principal stresses is shown in figure 12. We can see that under external loading before sintering all the three stress components are nearly equal which is expected since we should have the state of hydrostatic compression. With the progress of sintering the radial stresses gradually decrease to zero due to radial shrinkage of the specimen and finally the state of uniaxial compression is obtained.

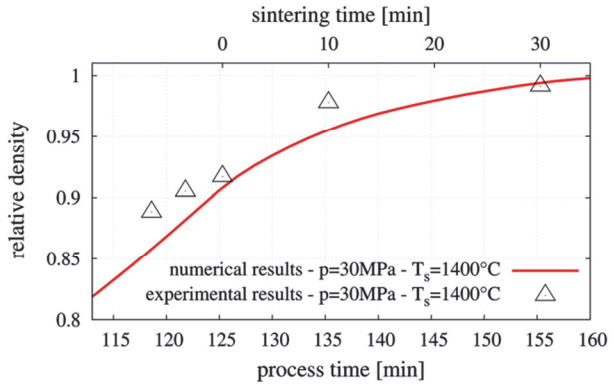

Fig. 10. *Density evolution during sintering.*

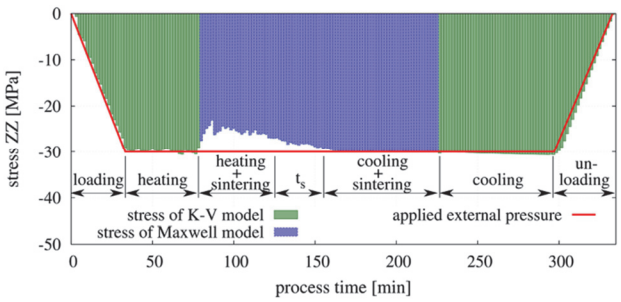

Fig. 11. *Evolution of macroscopic axial stresses during the whole process.*

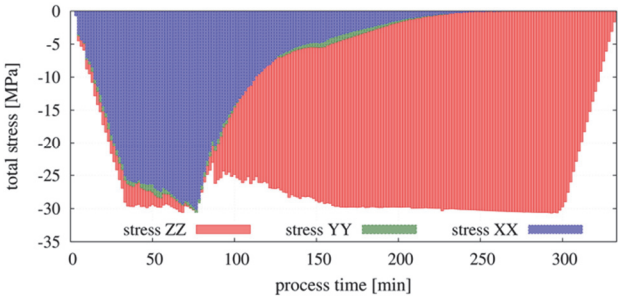

Fig. 12. *Evolution of macroscopic axial stresses during the whole process.*

7. CONCLUDING REMARKS

The results presented in this paper show that the micromechanical model of sintering developed within the framework of the discrete element method reproduces correctly macroscopic behaviour of the material during sintering. The macroscopic stresses and other macroscopic quantities can be obtained by upscaling of the microscopic parameters. This will allow to use the discrete element model for multiscale modelling of sintering.

ACKNOWLEDGEMENTS

The results presented in this paper have been obtained within the projects funded by the National Science Centre awarded by decision numbers DEC-2013/11/B/ST8/03287, DEC-2012/05/N/ST8/03376 and DEC-2014/12/T/ST8/00681, as well as Operational Programme Human Capital 8.2.1.

REFERENCES

Chang, Ch.S., Chao, S.J., Chang, Y., 1995, Estimates of Elastic Moduli for Granular Material with Anisotropic Random Packing Structure, *Int J Solids Struct*, 32, 1989–2008.

Coble, R.L., 1961, Sintering of Crystalline Solids. I. Intermediate and Final State Diffusion Models, J Appl Phys, 32, 787-792.

De Jonghe, L.C., Rahaman, M.N., 1988, Sintering Stress of Homogeneous and Heterogeneous Powder Compacts, *Acta Metall Mater*, 36, 223-229.

Dempack, 2013, DEMpack – discrete/finie elements simulation software, www.cimne.com/dem (access: November 2014).

Johnson, D.L., 1969, New Method of Obtaining Volume, Grain Boundary and Surface Diffusion Coefficients from Sintering Data, *J Appl Phys*, 40, 192-200.

Kruyt, N.P., Rothenburg, L., 1998, Statistical Theories for the Elastic Moduli of Two-Dimensional Assemblies of Granular Materials, *Int J Eng Sci*, 36, 1127-1142.

Kruyt, N.P., Rothenburg, L., 2004, Kinematic and Static Assumptions for Homogenization in Micromechanics of Granular Materials, *Mech Mater*, 36, 1157-1173.

Luding, S., 2004, Micro-Macro Transition for Anisotropic, Frictional Granular Packings, *Int J Solids Struct*, 41, 5821–5836.

Martin, C.L., Schneider, L.C.R., Olmos, L., Bouvard, D., 2006, Discrete Element Modeling of Metallic Powder Sintering, *Scripta Mater*, 55, 425-428.

Nosewicz, S., Rojek, J., Pietrzak, K., Chmielewski, M., 2013, Viscoelastic Discrete Element Model of Powder Sintering, *Powder Technol*, 246, 157-168.

Olevsky, E.A., 1998, Theory of Sintering: From Discrete to Continuum, *Mat Sci Eng R*, 23, 41-100.

Olmos, L., Martin, C.L., Bouvard, D., 2009, Sintering of Mixtures of Powders: Experiments and Modelling, *Powder Technol*, 190, 134-140.

Pan, J., 2003, Modelling Sintering at Different Length Scales, *Int Mater Rev*, 2, 69-85.

Parhami, F., McMeeking, R.M., 1998, A Network Model for Initial Stage Sintering, *Mech Mater*, 27, 111-124.

Rojek, J., Zarate, F., Agelet de Saracibar, C., Gilbourne, Ch., Verdot, P., 2005, Discrete Element Modelling and Simulation of Sand Mould Manufacture for the Lost Foam Process, *Int J Numer Meth Eng*, 62, 1421-1441.

Taylor, L.M., Preece, D.S., 1992, Simulation of Blasting Induced Rock Motion, *Eng Computation*, 9, 243-252.

WYZNACZANIE NAPRĘŻEŃ MAKROSKOPOWYCH W DYSKRETNYM MODELU SPIEKANIA

Streszczenie

Artykuł przedstawia analizę naprężeń makroskopowych w procesie metalurgii proszków modelowanym metoda elementów dyskretnych. Metoda elementów dyskretnych należy do metod modelowania mikromechanicznego. W tej metodzie materiał jest reprezentowany przez liczny zbiór cząstek oddziałujących między sobą poprzez siły kontaktu. Sformułowanie metody wykorzystuje związki pomiędzy siłami i przemieszczeniami.

Wyznaczenie naprężeń makroskopowych wymaga zastosowania procedury przejścia między poziomem mikro- i makroskopwym. W artykule przedstawione jest podstawowe sformułowanie metody elementów dyskretnych ze szczególną uwagą zwróconą na modele oddziaływania kontaktowego proszku poddanego prasowaniu i spiekaniu. Przedstawiono metodę obliczania naprężeń makroskopowych wykorzystującą dwuetapowe uśrednianie. Dyskretny model spiekania jest zweryfikowany poprzez porównanie z własnymi wynikami doświadczalnymi spiekania proszku NiAl. Naprężenia makroskopowe są obliczone dla całego procesu obejmującego prasowanie, grzanie, spiekanie, chłodzenie i odciążenie. Stwierdzono zgodność naprężeń ze zmiennymi parametrami procesu. Opracowana procedura może być wykorzystana w wieloskalowym modelowaniu procesu spiekania.

Received: November 27, 2014
Received in a revised form: December 17, 2014
Accepted: December 19, 2014